Degradation Data-Driven Time-To-Failure Prognostics Approach for Rolling Element Bearings in Electrical Machines

Jun Wu, Chaoyong Wu, Shuai Cao, Siu Wing Or, Chao Deng and Xinyu Shao

Abstract —Time-to-failure (TTF) prognostics plays a crucial role in predicting remaining lifetime of electrical machines for improving machinery health management. This paper presents a novel three-step degradation data-driven TTF prognostics approach for rolling element bearings (REBs) in electrical machines. In degradation feature extraction step, multiple degradation features, including statistical features, intrinsic energy features, and fault frequency features, are extracted to detect the degradation phenomenon of REBs using complete ensemble empirical mode decomposition with adaptive noise and Hilbert-Huang transform methods. In degradation feature reduction step, the degradation features, which are monotonic, robust, and correlative to the fault evolution of the REBs, are selected and fused into a principal component Mahalanobis distance health index using dynamic principal component analysis and Mahalanobis distance methods. In TTF prediction step, the degradation process and local TTF of the REBs are observed by an exponential regression-based local degradation model, and the global TTF is predicted by an empirical Bayesian algorithm with a continuous update. A practical case study involving run-to-failure experiments of REBs on PRONOSTIA platform is provided to validate the effectiveness of the proposed approach and to show a more accurate prediction of TTF than the existing major approaches.

Index Terms—Degradation data-driven approach, degradation feature, electrical machines, rolling element bearings, time-to-failure prognostics.

I. INTRODUCTION

ROLLING element bearings (REBs) are an extremely critical component in electrical machines to constrain relative motions to the desired motion while reducing frictions between moving parts. REB failure is one of the foremost causes of failure in electrical machines, accounting for 45–55% of breakdown in asynchronous motors [1]. Time to failure (TTF) is defined as the time of which failure threshold is reached. It has become increasingly important and urgent for condition monitoring, remaining lifetime prediction, and operation optimization over the past decade [2]. The ability to accurately prognosticate the TTF of REBs is scientifically interesting and technically important to avoid their sudden failures, minimize machinery downtime, and improve machinery healthy management.

TTF prognostics can generally be classified into two main types: namely, model-based methods and data-driven methods. Model-based methods use mathematical models to represent physics of failures and phenomenon of degradation. They are only suitable for TTF prognostics when accurate failure mechanism models can be built. In fact, it is extremely difficult to build such an accurate failure mechanism model in many industrial applications because failures are usually unique to operating environments and model parameters are often unavailable [3]. Data-driven methods are more generic in that they directly use condition monitoring (CM) data to infer the future progress of failures and to predict the corresponding TTFs without any assumption on the underlying failure mechanism. A data-driven method for predicting the remaining useful life of REBs has been introduced using extended Kalman filter (KF), which relies on both time and time-frequency domain features to track the evolution of REB faults [4]. A new data-driven feature extraction/selection method for prognostics has been reported to map raw vibration data into monotonic features with early trends [5]. An on-line TTF prediction method for multi-sensor dynamic systems under latent degradation has been proposed using Wiener process and distributed KF [6]. In general, there are two important steps to realize data-driven methods in TTF prognostics. These include: 1) useful features extraction and reduction for learning

Jun Wu, Chaoyong Wu, and Shuai Cao are with School of Naval Architecture and Ocean Engineering, Huazhong University of Science and Technology and with Collaborative Innovation Center for Advanced Ship and Deep-Sea Exploration, Wuhan 430074, China, (e-mails: wuj@hust.edu.cn; woocy@hust.edu.cn; cs940823@163.com)

Siu Wing Or is with Department of Electrical Engineering, The Hong Kong Polytechnic University, Hung Hom, Kowloon, Hong Kong and with Hong Kong Branch of National Rail Transit Electrification and Automation Engineering Technology Research Center, Hong Kong (e-mail: eeswor@polyu.edu.hk)

Chao Deng and Xinyu Shao are with National Engineering Research Center of Digital Manufacturing Equipment, Huazhong University of Science and Technology, Wuhan 430074, China (e-mails: dengchao@hust.edu.cn; shaoxy@hust.edu.cn)

Corresponding author contacts, phone: +86 027 87543258, fax: +86 027 87542146, e-mail: wuj@hust.edu.cn; shaoxy@hust.edu.cn.

degradation behavior; and 2) future behavior prognostics for predicting TTF and its uncertainty.

For useful features extraction and reduction, time-domain, frequency-domain, and time-frequency analyses are the three main feature extraction methods. Time-domain analysis extracts features like kurtosis and skewness to detect the degradation states of REBs. Frequency-domain analysis is used to identify frequency components of REBs by fast Fourier transform. Popular time-frequency analysis methods such as wavelet transform, empirical mode decomposition (EMD), and Hilbert-Huang transform (HHT) [7] are used to extract health indicators from vibration signals and track the degradation of REBs. However, useful feature extraction is still arduous due to inherent nonlinearity and weak degradation characteristics of CM data. Hence, the dimensionality of extracted features are reduced by principal component analysis (PCA) [8], partial least square [9], self-organizing map methods [10], etc.

For future behavior prognostics, the reduced features are employed to train prediction models for the estimation of the TTF and its uncertainty. Statistical and machine learning methods, such as stochastic processes [11], hidden Markov models (HMM) [12], Bayesian networks [13], neural networks [14], and support vector machines (SVM) [15], are adopted to build the prediction models. Those methods offer a tradeoff between accuracy, complexity, and applicability.

While useful, there exist two main deficiencies in using data-driven methods. First, the strong dependence of the prediction accuracy of most data-driven methods on the quantity of CM data and the quality of extracted features imposes critical challenges on industrial applications. Second, the arduously revealed underlying degradation mechanisms prevent the effectiveness and efficiency of TTF prediction.

In this paper, we propose a three-step degradation data-driven TTF prognostics approach for REBs, comprising degradation feature extraction (step 1), degradation feature reduction (step 2), and TTF prognostics (step 3). The proposed approach automatically extracts and reduces a series of degradation features from collected vibration signals and continuously updates the TTF prediction. For this purpose, multiple degradation features are extracted to detect the degradation phenomenon of the REBs using statistical analysis, complete ensemble empirical mode decomposition with adaptive noise (CEEMDAN) [16], and HHT methods. The corresponding degradation features are selected by analyzing their monotonicity, robustness, and correlation. They are then fused by dynamic principal component analysis (DPCA) and Mahalanobis distance to give a principal component Mahalanobis distance (PCMD) health index of the REBs. An exponential regression-based local degradation model is constructed to observe the degradation process and to obtain the local TTF. An empirical Bayesian algorithm is introduced to predict the global TTF of the REBs based on the local TTF observations. The main contributions of this paper include: 1) multiple degradation features are extracted by integrated time-domain, frequency-domain, time-frequency analyses to discover useful degradation features; 2) a PCMD health index is found to represent the REB degradation mechanism over time using DPCA and Mahalanobis distance; and 3) a new degradation data-driven TTF prognostics approach is created

with the continuous update to provide a more accurate prediction of TTF using exponential regression and empirical Bayesian algorithm.

The paper is organized to have four sections. Section II presents the framework of the proposed degradation data-driven TTF prognostics approach. Section III provides a practical experimental study of REBs for validating the effectiveness of the proposed approach and for demonstrating a more accurate prediction of TTF than the existing major approaches. Section IV gives the conclusion of present work.

II. FRAMEWORK OF PROPOSED DEGRADATION DATA-DRIVEN TTF PROGNOSTICS APPROACH

Fig. 1 shows the framework of the proposed degradation data-driven TTF prognostics approach for REBs. The approach consists of three main steps as follows:
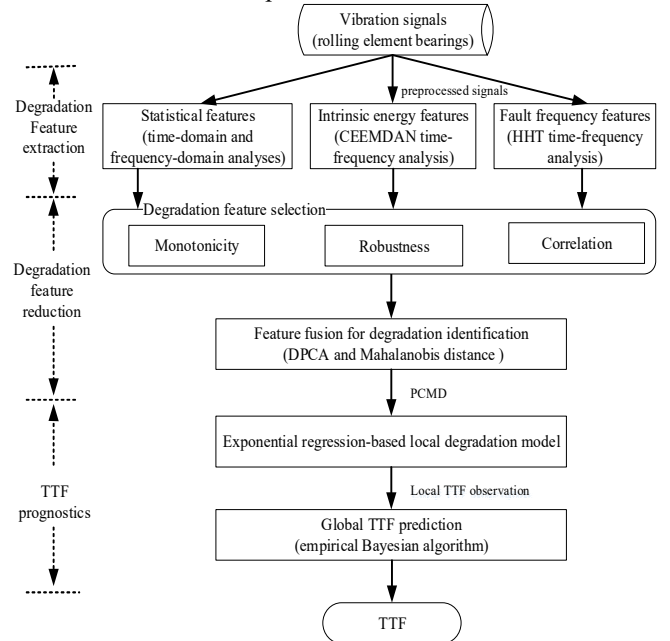
Fig. 1. Framework of degradation data-driven TTF prognostics approach for REBs.

(1) Degradation features extraction: This first step is aimed to extract multiple degradation features, including statistical features, intrinsic energy features, and fault frequency features. The statistical features are computed by time-domain and frequency-domain analyses. The intrinsic energy features and fault frequency features are calculated by CEEMDAN and HHT time-frequency analyses, respectively.

(2) Degradation feature reduction: This second step is aimed to discover the PCMD health index for the REBs by selecting and fusing the extracted degradation features. A degradation feature subset is constructed by analyzing their monotonicity, robustness, and correlation to fault evolution of the REBs. DPCA and Mahalanobis distance methods are introduced to obtain the PCMD health index and to identify the initial degradation time.

(3) TTF prognostics: This third step is aimed to continuously update and predict the TTF of the REBs. An exponential regression-based local degradation model is built to represent the local degradation trajectory and to provide an observation of the local TTF. An empirical Bayesian algorithm

is adopted to enable an accurate prediction of the global TTF in light of the local TTF observations.

A. Step 1: Degradation Feature Extraction

After raw vibration signals are collected from REBs and preprocessed using singular value elimination and Kalman filtering methods, multiple degradation features will be extracted in order to detect the degradation phenomenon of REBs and to track their time evolution.

1) Statistical features extracted by time-domain and frequency-domain analyses

In time domain, there are 8 statistical features covering a wide range of popular time-domain characteristics to be extracted from the preprocessed vibration signals, namely mean value (MV), root mean square value (RMSV), maximum absolute value (MAV), square mean root value (SMRV), skewness coefficient (SC), kurtosis coefficient (KC), shape factor (SF), and clearance factor (CF) [7]. The features of MV, RMSV, MAV, and SMRV indicate the amplitude and energy over the time domain of the signal, while those of SC, KC, SF, and CF reflect the distribution situation over the time domain. In frequency domain, there are 2 statistical features describing the change in frequency components to be extracted by power spectrum density analysis, including root mean square frequency (RMSF) and root variance frequency (RVF). The two features indicate the variation of main frequency band and the dispersion of spectral energies of the vibration signal. Table I summarizes the 10 statistical features, where N is the number of sampling points.

TABLE I
10 STATISTICAL FEATURES OF REBS

Feature	Equation
MV	$X_{mv} = \dfrac{1}{N}\sum_{i=1}^{N} X(t_i)$
RMSV	$X_{rmsv} = \sqrt{\dfrac{1}{N}\sum_{i=1}^{N} X^2(t_i)}$
MAV	$X_{mav} = \max\big(X(t_i)\big)$
SMRV	$X_{smrv} = \left[\dfrac{1}{N}\sum_{i=1}^{N} \sqrt{|X(t_i)|}\right]^2$
SC	$X_{sc} = \dfrac{1}{X_{rms}{}^3}\sum_{i=1}^{N} (X(t_i) - X_{mv})^3$
KC	$X_{kc} = \dfrac{1}{X_{rms}{}^4}\sum_{i=1}^{N} (X(t_i) - X_{mv})^4$
SF	$X_{sf} = \dfrac{X_{rms}}{\frac{1}{N}\sum_{i=1}^{N}|X(t_i)|}$
CF	$X_{cf} = \dfrac{X_{mav}}{X_{rms}}$
RMSF	$X_{rmsf} = \sqrt{\dfrac{\sum_{i=2}^{N}\dot{X}^2(t_i)}{4\pi^2\sum_{i=1}^{N}X^2(t_i)}}$
RVF	$X_{rvf} = \sqrt{\dfrac{\sum_{i=2}^{N}\dot{X}^2(t_i)}{4\pi^2\sum_{i=1}^{N}X^2(t_i)} - \big(\dfrac{\sum_{i=2}^{N}\sum_{i=2}^{N}\dot{X}(t_i)X(t_i)}{2\pi\sum_{i=1}^{N}X^2(t_i)}\big)^2}$

2) Intrinsic energy features extracted by CEEMDAN

CEEMDAN is the latest version of EMD algorithm for signal processing in time-frequency domain. It is capable of self-adaptively decomposing complex vibration signals into a number of intrinsic mode functions (IMFs) and a residue. The IMFs illustrate the natural oscillatory mode embedded in the signals. When the degradation of REBs occurs, the corresponding resonance frequency components will be produced in the signals, and the intrinsic energy in the IMFs will change accordingly. The intrinsic energy of REB faults is larger than the normal one so that the intrinsic energy features are extracted from the vibration signals using CEEMDAN. Given a preprocessed vibration signal $X(t)$, the procedure of the CEEMDAN-based intrinsic energy feature extraction is described below.

a) By adding a white noise time series $W_i(t)$ with zero mean and unity variance into $X(t)$, a new signal $X_i(t)$ is generated as

$$X_i(t) = X(t) + \varepsilon_k W_i(t), \quad i = 1, 2, \dots, I \tag{1}$$

where I is the ensemble number and ε_k is coefficient.

b) $X_i(t)$ is decomposed using empirical mode decomposition to obtain the first IMF $E_1(X_i(t))$ and its mean $\widehat{IMF}_1(t)$ as

$$\widehat{IMF}_1(t) = \frac{1}{I}\sum_{i=1}^{I} E_1(X_i(t)). \tag{2}$$

c) A residue $r_1(t)$ is calculated and expressed as

$$r_1(t) = X(t) - \widehat{IMF}_1(t). \tag{3}$$

d) The decomposition will stop if $r_1(t)$ is monotonic. Otherwise, a new signal $X_{1i}(t)$ is generated by adding an adaptive white noise to $r_1(t)$, giving

$$X_{1i}(t) = r_1(t) + \varepsilon_1 E_1(W_i(t)). \tag{4}$$

e) Following the above steps, the mean of the second IMF $\widehat{IMF}_2(t)$ is obtained as

$$\widehat{IMF}_2(t) = \frac{1}{I}\sum_{i=1}^{I} E_1\left(r_1(t) + \varepsilon_1 E_1(W_i(t))\right). \tag{5}$$

In the same way, all the IMFs and final residue of the signal $X(t)$ will be obtained. The original signals can be acquired by the sum of all IMFs and the final residue as

$$X(t) = \sum_{j=1}^{J} \widehat{IMF}_j(t) + r(t), \tag{6}$$

where J is the IMF number.

f) The final residual signal $r(t)$ is regarded as $(k+1)$th IMF. The intrinsic energy features of REBs are defined as

$$\text{IEF}\big[\widehat{IMF}_j(t)\big] = [1/(N-1)]\sum_{i=1}^{N}\big[\widehat{IMF}_j(t_i)\big]^2, \tag{7}$$

where N is the sampling point.

3) Fault frequency features extracted by HHT

During the operation of REBs, any kind of degradation (e.g., outer ring, inner ring, element, cage, etc.) may occur. Once degradation occurs, there will have high-frequency shock vibrations in the REB operation. HHT is another useful time-frequency analysis method to accurately provide the changing rule of the amplitude of the high-frequency shock vibration signals with frequency and time [17]. The HHT time-frequency analysis is adopted to extract the fault frequency features of REBs. The procedure of HHT-based fault frequency feature extraction is described as follows.

a) Preprocessed vibration signals of REBs is adaptively decomposed using CEEMDAN-based intrinsic energy feature extraction to obtain IMFs, denoted as $\widehat{IMF}_k(t)$, $k = 1, \cdots, n$.

b) Hilbert transform is applied to $\widehat{IMF}_k(t)$ and $\widehat{IMF}_i(t)$, giving

$$\widehat{IMF}_i(t) = \frac{1}{\pi}\int_{-\infty}^{\infty} \frac{\widehat{IMF}_k(t)}{t-\tau} d\tau. \tag{8}$$

The analytical form of $\widehat{IMF}_k(t)$, denoted $z_i(t)$, is written as

$$z_i(t) = \widehat{IMF}_k(t) + j\widehat{IMF}_i(t) = a_i(t)e^{j\phi_i(t)}, \tag{9}$$

where $a_i(t)$ and $\phi_i(t)$ are the instantaneous amplitude and phase of $\widehat{IMF}_k(t)$, respectively. They can be formulated as

$$\begin{cases} a_i(t) = \sqrt{\widehat{IMF_l}^2(t) + \widehat{IMF_k}^2(t)} \\ \emptyset_i(t) = \arctan \frac{\widehat{IMF_l}}{\widehat{IMF_k}} \end{cases} \tag{10}$$

c) The instantaneous frequency $f_i(t)$ is obtained from the instantaneous phase as

$$f_i(t) = \frac{1}{2\pi}\omega_i(t) = \frac{1}{2\pi}\frac{d\emptyset_i(t)}{dt}. \tag{11}$$

d) The Hilbert spectral density is expressed as

$$H_i(\omega,t) = RP \sum_{i=1}^{n} a_i(t)e^{j\emptyset_i(t)}, \tag{12}$$

where RP is real number.

e) The Hilbert marginal spectrum is obtained as

$$h_i(\omega) = \int_0^T H(\omega,t)dt. \tag{13}$$

f) According to the characteristic frequencies of different components of REBs, the fault frequency features (FFF) of REBs are extracted from the Hilbert marginal spectrum using

$$FFF \rightarrow \max[h_i(f_0, f_i, f_b, f_c)], \tag{14}$$

where f_o is the outer ring frequency, f_i is the inner ring frequency, f_b is the rolling element frequency, and f_c is the cage frequency. They are expressed as

$$\begin{cases} f_i = \frac{N_b}{2} \cdot f_r \cdot \left[1 + \frac{D_b}{D_p} \cdot \cos\varphi\right] \\ f_o = \frac{N_b}{2} \cdot f_r \cdot \left[1 - \frac{D_b}{D_p} \cdot \cos\varphi\right] \\ f_b = \frac{D_b}{D_p} \cdot f_r \cdot \left[1 - \frac{D_b^2}{D_p^2} \cdot \cos^2\varphi\right] \\ f_c = \frac{1}{2} \cdot f_r \cdot \left[1 - \frac{D_b}{D_p} \cdot \cos\varphi\right] \end{cases} \tag{15}$$

where f_r is the rotation frequency, φ is the contact angle, N_b is the number of rolling-element elements, D_b is the diameter of rolling-element element, and D_p is the pitch diameter.

B. Step 2: Degradation Feature Reduction

Since some extracted degradation features may not be related to the degradation phenomenon of REBs, they may not be able to indicate the variation until failure occurs. To increase the effectiveness and efficiency of TTF prognostics, it is required to have selection from the extracted degradation features as well as to reveal the PCMD health index for REBs by fusing the selected degradation features.

1) Degradation feature selection

Reasonable degradation features are well correlated with item degradation processing, monotonically increasing or decreasing, and robust to outliers [18]. The monotonicity, robustness, and correlation of the extracted degradation features are estimated to pick up a degradation feature subset. The procedure of degradation feature selection is as follows:

a) An extracted degradation feature is decomposed into its mean trend and random part using smoothing method as

$$f(t_k) = f_T(t_k) + f_R(t_k), \tag{16}$$

where $f(t_k)$ is feature value at time t_k, $f_T(t_k)$ is the trend value, and $f_R(t_k)$ is the residual value.

b) The metrics of the monotonicity (Mon), robustness (Rob), and correlation ($Corr$) of the extracted degradation features are written as

$$\begin{cases} Mon(f) = \frac{1}{K-1}\left|\sum_k \delta(f_T(t_{k+1}) - f_T(t_k)) - \sum_k \delta(f_T(t_k) - f_T(t_{k+1}))\right| \\ Rob(f) = \frac{1}{K}\sum_k \exp\left(-\left|\frac{f_R(t_k)}{f(t_k)}\right|\right) \\ Corr(f) = \frac{|K\sum_k f_T(t_k)t_k - K\sum_k f_T(t_k)\sum_k t_k|}{\sqrt{[K\sum_k f(t_k)^2 - (\sum_k f_T(t_k))^2][K\sum_k t_k^2 - (\sum_k t_k)^2]}} \end{cases} \tag{17}$$

where K is the total number of the sampling points and $\delta(\cdot)$ is the simple unit step function.

c) A weighted linear combination of the metrics is defined as the degradation feature selection criteria. This is because one metric only partially measures the suitability of a candidate for TTF prognostics and feature selection only based on one metric will be biased. The formula is

$$\max_{T\in\Omega} Z = \omega_1 Mon(f) + \omega_2 Rob(f) + \omega_3 Corr(f)$$
$$s.t., \sum_{i=1}^{3}\omega_i = 1, \quad \omega_i > 0 \tag{18}$$

where Z is the objective to be optimized, Ω is the universal set of all candidate features, and ω_i is the weighted coefficient. It is noted from mathematical derivation that the comprehensive objective Z is linearly and positively correlated with each metric so that Z is also positively correlated with the selected degradation features and the features of high Z score should be selected.

2) Feature fusion for degradation identification

Due to the fact that the selected degradation features of REBs are still high dimensional, a PCMD health index is found by way of feature fusion using DPCA and Mahalanobis distance methods [19]. The proposed PCMD health index evaluates the similarity of first principal components (PCs) by comparing Mahalanobis distance between these latter. This shows the degradation time evolution of REBs. The procedure of the feature fusion is described as follows:

a) The matrix F of the selected n-dimensional degradation features of REBs is structured to be

$$F = \begin{bmatrix} f_{11} & f_{12} & \cdots & f_{1n} \\ f_{21} & f_{22} & \cdots & f_{2n} \\ \vdots & \vdots & \ddots & \vdots \\ f_{m1} & f_{m2} & \cdots & f_{mn} \end{bmatrix} = (F_1, F_2, \cdots, F_n) \tag{19}$$

where $F_i = (f_{1i}, f_{2i}, \cdots, f_{mi})^T$ is ith normalized feature vector and contains m observed values.

b) According to DPCA method, the matrix F is transformed to obtain a score matrix T as

$$T = A^T F \tag{20}$$

where $A = (A_1, A_2, \cdots, A_n)$ is the transform matrix which comprises eigenvectors $A_i = (a_{i1}, a_{i2}, \cdots, a_{im})$ corresponding to the largest eigenvalues λ_i for the correlation matrix of F. The projected vectors in the score matrix T are the PCs for defining the PCMD index.

c) The proposed PCMD health index is expressed as

$$PCMD_j = \sum_{i=1}^{n} \lambda_{0i}\lambda_i\sqrt{(T_{ij} - \mu)^T S^{-1}(T_{ij} - \mu)}, \tag{21}$$

where $PCMD_j$ is the PCMD index of jth sampling, T_{*j} is the first PCs of current REB, and μ and S are the mean and covariance of the PCs of normal REBs, respectively. It is not arduous to find the degradation time of REBs in accordance with the obtained PCMD health index.

C. Step 3: TTF Prognostics

The proposed TTF prognostics is implemented from the beginning of the degradation identified in Section B. It involves two main steps: namely, local degradation model based on exponential regression and global TTF prediction based on empirical Bayesian algorithm.

1) Local degradation model based on exponential regression

There are many factors affecting the degradation of REBs, and the degradation mechanics are very difficult to be established. A simple regression curve is not able to fit with the global degradation trajectory of REBs. By regarding several successive PCMD health indexes as a local degradation sequence, however, the local degradation model of a sub-sequence can be built. Thus, exponential regression is adopted by us to fit with the local degradation trajectory as it is very suitable for the representation of degradation [20].

As shown in Fig. 2, $PCMD_k$ represents the PCMD health index at the moment of t_k and $PCMD_{q:k}$ denotes a sequence of PCMD health indexes from the moment of t_q to t_k, $q = 1, \dots, k - q_0 + 1$, and q_0 is the least number for exponential regression. For the moment of t_k, the local degradation sequence includes $PCMD_{1:k}, PCMD_{2:k}, \dots, PCMD_{k-q_0+1:k}$ and is used to fit with the local degradation trajectory using exponential regression as

$$PCMD_k = \alpha * \exp(\beta t_k), \tag{22}$$

where α and β are the parameters to be estimated by least square algorithm [9]. Herein, the number of the obtained local degradation trajectory at the moment of t_k is $k - q_0 + 1$. In order to assess how appropriate each local degradation trajectory describes the actual degradation, mean square error of the PCMD health indexes in regression and prediction is calculated as

$$\begin{cases} RD_{q:k} = \sum_{i=q}^{k} \left(\widehat{PCMD}_i - PCMD_i \right)^2 / (k - q + 1) \\ PD_{q:k} = \left(\widehat{PCMD}_{k+1} - PCMD_{k+1} \right)^2 \end{cases} \tag{23}$$

where $RD_{q:k}$ represents the mean square error of the $PCMD_{q:k}$ in regression, $PD_{q:k}$ denotes the mean square error of the $PCMD_{q:k}$ in prediction, and $\widehat{PCMD}_i$ indicates the fitted value of the degradation sequences $PCMD_{q:k}$ at the moment of t_i.

By setting $r_{q:k}$ as the sum of $RD_{q:k}$ and $PD_{q:k}$, it can estimate the overall performance in the regression and prediction. The smaller $r_{q:k}$ is, the better the overall performance will be obtained. Meanwhile, a weight coefficient $\omega_{q:k}$ is calculated in accordance with $r_{q:k}$ to be

$$\begin{cases} r_{q:k} = RD_{q:k} + PD_{q:k} \\ \omega_{q:k} = \frac{1}{r_{q:k}} / \sum_{i=1}^{k-q_0+1} \frac{1}{r_{i:k}} \end{cases} \tag{24}$$

According to the obtained local degradation trajectory at the moment of t_k, the corresponding local TTF $\hat{t}_{q:k}, q = 1,2,\dots, k - q_0 + 1$ is calculated as

$$\hat{t}_{q:k} = \widehat{PCMD}_{q:k}^{-1}(PCMD_{FD}) \tag{25}$$

where $\widehat{PCMD}_{q:k}^{-1}$ represents the inverse function of $\widehat{PCMD}_{q:k}$ and $PCMD_{FD}$ denotes the fault threshold. The weight coefficient $\omega_{q:k}$ is assigned to $\hat{t}_{q:k}$. The mean and variance of $\hat{t}_{q:k}$ are calculated as

$$\begin{cases} \hat{t}_k = \sum_{q=1}^{k-q_0+1} \omega_{q:k} \hat{t}_{q:k} \\ \sigma_k^2 = \frac{\sum_{q=1}^{k-q_0+1} \omega_{q:k}(\hat{t}_{q:k}-\hat{t}_k)^2}{k-q_0+1} \end{cases} \tag{26}$$

where $\hat{t}_k$ is the local TTF observation at the moment of t_k and σ_k^2 is the observation error. The local TTFs at different times are constituted and denoted as $\hat{t}_{q_0+1:n}$.
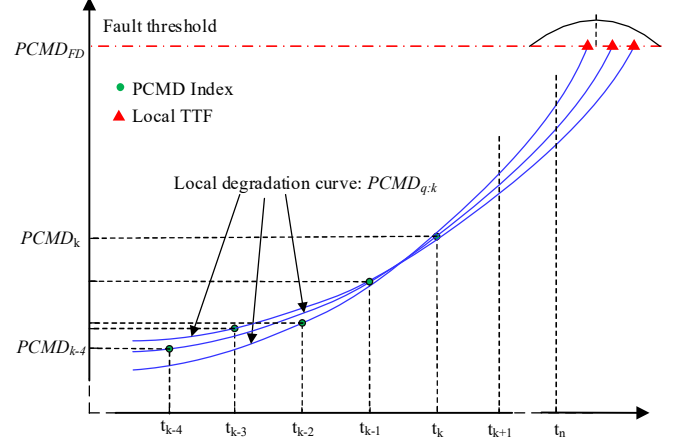
Fig. 2. Local degradation curve based on exponential regression.

2) TTF prediction based on empirical Bayesian algorithm

The local TTFs at different times are stochastic. Let $\hat{t}_{q_0+1:n}$ be a sample of a common prior distribution $\pi(\theta_k)$, which follows a normal distribution $N(\mu_z, \sigma_z^2)$ where μ_z and σ_z^2 are unknown hyper parameters. The empirical Bayesian algorithm is proposed to realize the global TTF prediction, including prior distribution estimation and posterior distribution estimation.

a) Prior distribution estimation

The local TTF $\hat{t}_k$ is the observation of θ_k, and σ_k^2 is used to measure the observation error. To eliminate the influence of dynamic fluctuations in the degradation of REBs, σ_f^2 is set to the mean of σ_k^2 and is expressed as

$$\sigma_f^2 = \frac{\sum_{k=q_0+1}^{n} \sigma_k^2}{n-q_0}. \tag{27}$$

According to empirical Bayesian algorithm [21], [22], the joint distribution of $\hat{t}_k$ and θ_k is written as

$$\begin{aligned} h(\hat{t}_k, \theta_k) &= \pi(\theta_k) f(\hat{t}_k | \theta_k) \\ &= (2\pi\sigma_f\sigma_z)^{-1} \exp\left\{ -\frac{1}{2}\rho_k[\theta_k - \frac{1}{\rho_k}(\frac{\mu_z}{\sigma_z^2} + \frac{\hat{t}_k}{\sigma_f^2})] \right\} \exp\left\{ -\frac{(\mu_z - \hat{t}_k)^2}{2(\sigma_z^2 + \sigma_f^2)} \right\} \end{aligned} \tag{28}$$

where ρ_k is the sum of σ_z^{-2} and σ_f^{-2} and $f(\hat{t}_k | \theta_k)$ is the conditional probability of $\hat{t}_k$ based on θ_k.

The marginal distribution of $\hat{t}_k$ is computed using

$$\begin{aligned} m(\hat{t}_k) &= \int_{-\infty}^{+\infty} \pi(\theta_k) f(\hat{t}_k | \theta_k) d\theta_k = (2\pi\rho_k)^{-\frac{1}{2}}(\sigma_f\sigma_z)^{-1} \\ &\exp\left\{ -\frac{(\hat{t}_k - \mu_z)^2}{2(\sigma_z^2 + \sigma_f^2)} \right\} \end{aligned} \tag{29}$$

it follows a normal distribution $N(\mu_z, (\sigma_z^2 + \sigma_f^2))$.

Thus, the likelihood function of $\hat{t}_{q0+1}, \dots, \hat{t}_n$ is counted as

$$m(\hat{t}_{q0+1}, \dots, \hat{t}_n) = [2\pi(\sigma_z^2 + \sigma_f^2)]^{-\frac{n-q_0}{2}} \exp\left\{ -\frac{(n-q_0)s^2}{2(\sigma_z^2+\sigma_f^2)} - \frac{(n-q_0)(\hat{\mu}_k-\mu_z)^2}{2(\sigma_z^2+\sigma_f^2)} \right\} \tag{30}$$

where $\hat{\mu}_k = \frac{\sum_{k=q_0+1}^{n}\hat{t}_k}{n-q_0}$, $s^2 = \sum_{k=q_0+1}^{n}(\hat{t}_k - \hat{\mu}_k)^2/(n-q_0)$. $m(\hat{t}_k)$ will be maximized when μ_z is $\hat{\mu}_k$ without thinking of $\sigma_k{}^2$. $\hat{\mu}_k$ is always at the maximum likelihood estimation of $\hat{t}_k$. The problem of maximum likelihood is simplified to the maximize function of $\sigma_z{}^2$ as

$$\varphi(\sigma_z{}^2) = (\sigma_z{}^2 + \sigma_f{}^2)]^{-\frac{n-q_0}{2}}\exp\left\{-\frac{(n-q_0)s^2}{2(\sigma_z{}^2+\sigma_f{}^2)}\right\} \quad (31)$$

Equation (31) can be transformed to be

$$\frac{d}{d\sigma_z{}^2}\log\varphi(\sigma_z{}^2) = \frac{-(n-q_0)}{2(\sigma_z{}^2+\sigma_f{}^2)} + \frac{(n-q_0)s^2}{2(\sigma_z{}^2+\sigma_f{}^2)} \quad (32)$$

when $s^2 \geq \sigma_f{}^2$, $\sigma_k{}^2 = s^2 - \sigma_f{}^2$ can maximize $\varphi(\sigma_z{}^2)$. Otherwise, when $s^2 < \sigma_f{}^2$, $\sigma_z{}^2 = 0$ can maximize $\varphi(\sigma_z{}^2)$. The unknown hyperparameters μ_z and $\sigma_z{}^2$ is deduced using

$$\begin{cases} \mu_z = \hat{\mu}_k \\ \sigma_z{}^2 = \max\left\{0, \frac{s^2}{n-q_0} - \sigma_f{}^2\right\} \end{cases} \quad (33)$$

Thus, the prior distribution estimation of θ_k follows a normal distribution $N(\mu_z, \sigma_z{}^2)$.

b) Posterior distribution estimation

Once the prior distribution is obtained, the posterior distribution is calculated as

$$\pi(\theta_k|\hat{t}_k) = \frac{h(\hat{t}_k, \theta_k)}{m(\hat{t}_k)}$$
$$= \sqrt{\frac{\rho_k}{2\pi}}\exp\left\{-\frac{1}{2}\rho_k[\theta_k - \frac{1}{\rho_k}(\frac{\mu_z}{\sigma_z{}^2} + \frac{\hat{t}_k}{\sigma_f{}^2})]^2\right\} \quad (34)$$

where $\pi(\theta_k|\hat{t}_k)$ is the density of $N(\mu(\hat{t}_k), V(\hat{t}_k))$. Considering that the number of the local TTF observations may be small, $\mu(\hat{t}_k)$ and $V(\hat{t}_k)$ can be adjusted as

$$\begin{cases} \mu^{EB}(\hat{t}_k) = \hat{t}_k - \hat{B}(\hat{t}_k - \hat{\mu}_z) \\ V^{EB}(\hat{t}_k) = \sigma_f{}^2\left(1 - \frac{p-1}{p}\hat{B}\right) - \frac{2}{p-3}\hat{B}^2(\hat{t}_k - \hat{\mu}_z)^2 \\ \hat{B} = \frac{p-3}{p-1} * \frac{\sigma_f{}^2}{\sigma_f{}^2+\hat{\sigma}_z{}^2} \\ \hat{\sigma}_z{}^2 = \sum_{k=q_0+1}^{n}(\hat{t}_k - \hat{\mu}_k)^2/(p-1) - \sigma_f{}^2 \end{cases} \quad (35)$$

Therefore, the posterior distribution of θ_k follows a normal distribution $N(\mu^{EB}(\hat{t}_k), V^{EB}(\hat{t}_k))$, which show the most probable TTF at the moment of t_k.

As discussed above, the posterior distribution of θ_k may be regarded as the global TTF prediction according to the PCMD health index sequence $PCMD_{1:n}$ expressed as

$$f(\theta_n|PCMD_{1:n}) = \pi(\theta_n|\hat{t}_k) \quad (36)$$

it follows a normal distribution $N(\mu^{EB}(\hat{t}_k), V^{EB}(\hat{t}_k))$.

III. EXPERIMENTS, RESULTS AND DISCUSSTION

A. Experimental Setup and Vibration Data

The degradation data of REBs was obtained from a laboratory experimental platform called PRONOSTIA [23] and was used to validate the effectiveness of the proposed approach and to show a more accurate prediction of TTF than the existing major approaches. Fig. 3 shows the overview of the PRONOSTIA platform.

Four tested REBs: namely, REB 1_1, REB 1_3, REB 2_1, and REB 2_2, were selected and analyzed because they showed degradation behaviors. A radial load force generated by a force actuator was applied to each REB in order to reduce its life duration. The run-to-failure experiments of REB 1_1 and REB

1_3 were performed at a radial load force of 4000 N and a shaft speed of 1800 rpm, while those of REB 2_1 and REB 2_2 were carried out using an increased radial load force of 4200 N and a reduced shaft speed of 1650 rpm. They indicate very different degradation behaviors leading to different experiment durations. The basic characteristics of these tested REBs are listed in Table Ⅱ. According to Equation (15), the fault frequencies of the inner race, outer race, rolling element, and cage of these tested REBs were calculated to be $f_i = 221$ Hz, $f_o = 168$ Hz, $f_b = 215.4$ Hz, and $f_c = 19$ Hz, respectively.
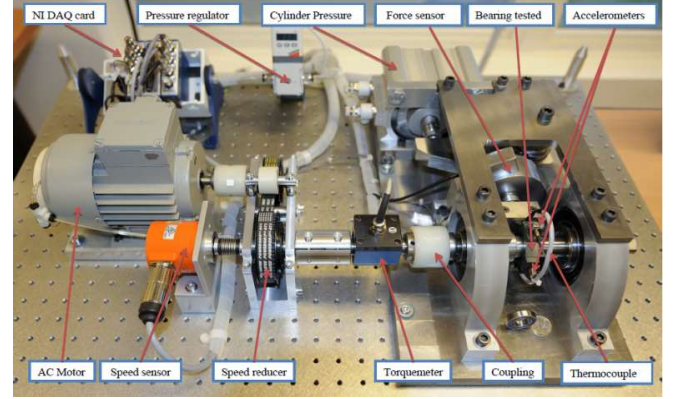
Fig. 3. The PRONOSTIA platform.

In the run-to-failure experiments, vibration signals were acquired by two high-frequency accelerometers (DYTRAN 3035B) mounted on the vertical and horizontal axes of the tested REBs. The sampling frequency of the vibration signals was set to 25.6 kHz, and a total of 2560 samples were recorded every 10 seconds. The sampling signals were logged by a computer for data storage and analysis via an NI DAQ card. The experiments would be stopped when the amplitude of the vibration signals exceeded 20 g.

TABLE Ⅱ
BASIC CHARACTERISTICS OF TESTED REBS

Design parameter	Value
Contact angle of the bearing (φ)	0°
Pitch diameter of the bearing (D_p)	25.6 mm
Diameter of rolling elements of the bearing (D_b)	3.5 mm
Number of rolling elements of the bearing(N_b)	13

The obtained vibration signals were preprocessed using singular value elimination and Kalman filtering methods to facilitate subsequent feature extraction. It is found that the vertical vibration signals give little useful information for the performance degradation of the REB. So, only the horizontal vibration signals are adopted for the TTF prognostics of the REBs in the following studies.

B. Degradation Feature Extraction

As described in Section II-A, 10 statistical features are firstly extracted. It is shown that among the statistical features, only MV, SC, and RVF are insensitive to the degradation phenomenon. Then, the intrinsic energy features of the tested bearings are extracted using CEEMDAN method. The decomposed components of the preprocessed vibration signals of REB 1_1 are derived from CEEMDAN method with $I = 100$ in Eq. (1). A total of 11 IMFs and a residue are obtained after the decomposition. The corresponding normalized intrinsic energy features are calculated according to the obtained IMFs.
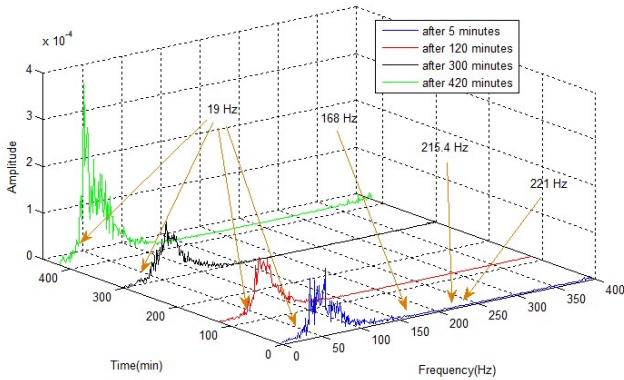
Fig. 4. Hilbert marginal spectrum of vibration signals of REB 1_1.
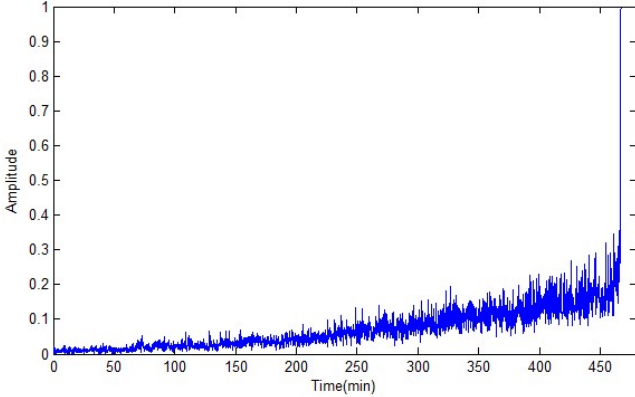
Fig. 5. Fault frequency feature of REB 1_1 derived from Fig. 4.

The fault frequency features of the tested REB are extracted using HHT method. Fig. 4 shows the Hilbert marginal spectrum of the vibration signals of REB 1_1. It is found that the magnitudes of the fault frequencies of the inner race, the outer race, the rolling element, and the cage all change over time. Fig. 5 plots the fault frequency feature of REB 1_1 based on Fig. 4. The extracted fault frequency feature indicates the degradation behavior over time.

C. Degradation Feature Reduction

There are 22 features extracted from the vibration signals of the tested REBs. However, some features do not indicate the degradation phenomenon. To improve the TTF prognostics performance, degradation feature reduction is implemented. Fig. 6 illustrates the monotonicity, robustness, and correlation of the extracted features for REB 1_1. Based on Fig. 6, Z score of the extracted features is calculated, and the extracted features with $Z \geq 0.6$ are selected and illustrated in Fig. 7. Statistical features (i.e., RMSV, MAV, SMRV, KC, SF, CF, and RMSF), intrinsic energy features (i.e., IEF3, IEF4, IEF5, IEF6, IEF7, and IEF9), and fault frequency features (i.e., FFF) are selected.
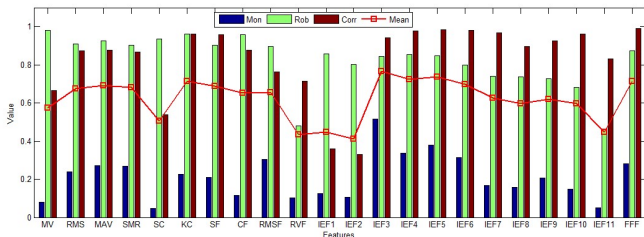
Fig. 6. Monotonicity, robustness, and correlation of REB 1_1.
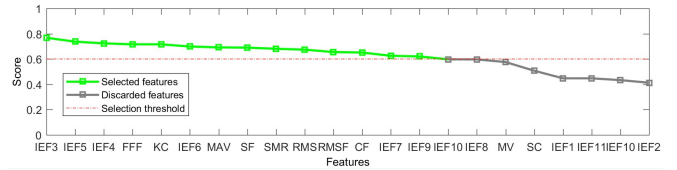
Fig. 7. Z score of the extracted features of REB 1_1.
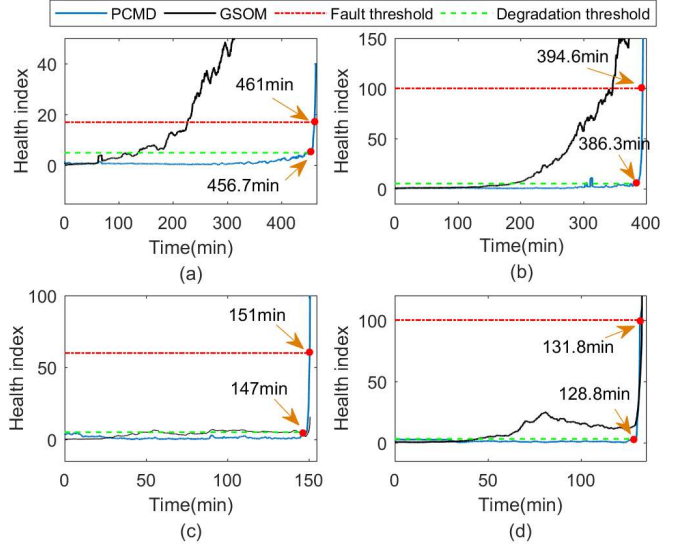
Fig. 8. PCMD health index for degradation identfication of (a) REB 1_1, (b) REB 1_3, (c) REB 2_1, and (d) REB 2_2.

Then, DPCA and Mahalanobis distance are introduced to fuse these selected features. The PCMD health index of the tested bearings is calculated and shown in Fig. 8. The degradation time of REB 1_1, REB 1_3, REB 2_1, and REB 2_2 is identified to be 456.7, 386.3, 147, and 128.8 min, respectively. The real TTF of REB 1_1, REB 1_3, REB 2_1, and REB 2_2 is to be 461, 394.6, 151, and 131.8 min, respectively. Fig. 8 clearly shows that PCMD health index may better represent the REB degradation mechanism over time than growing self-organizing map (GSOM) [24].

D. TTF Prognostics

As discussed in Section II-C, TTF prognostics of the tested REBs includes exponential regression-based local degradation model and empirical Bayesian-based global TTF prediction. Fig. 9 shows the local degradation curves of REB 1_1 at different sampling times of 458.3, 458.5, 459, 459.5, 460, and 460.5 min using exponential regression. The local TTF at the different sampling times is calculated to be 460.9, 459.8, 460.4, 461.1, 461.2, and 461.1 min. Fig. 10 shows the probability density function of local TTF at the different sampling times for REB 1_1, REB 1_3, REB 2_1, and REB 2_2. The local TTF distribution at different sampling times implicates the potential local degradation mechanics at the corresponding time.

The global TTF prediction is deduced by empirical Bayesian algorithm. Fig. 11 shows the global TTF prognostics and its 95% confidence interval from the beginning of the degradation of the tested bearings. The TTF prognostics starts with low accuracy due to the lack of training data. The accuracy becomes higher and higher over time. The final error of REB 1_1, REB 1_3, REB 2_1, and REB 2_2 is determined from Equation (37) to be 0.02, 0.86, 0.22, and 0.37, respectively. These error values are acceptable for major industrial applications.
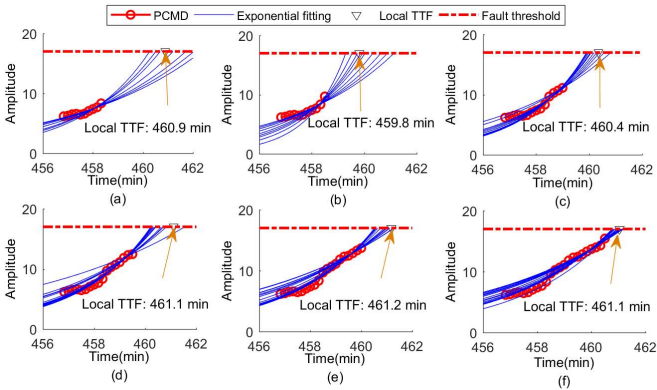
Fig. 9. Local degradation curves of REB 1_1 at different sampling times of (a) 458.3, (b) 458.5, (c) 459, (d) 459.5, (e) 460, and (f) 460.5 min.
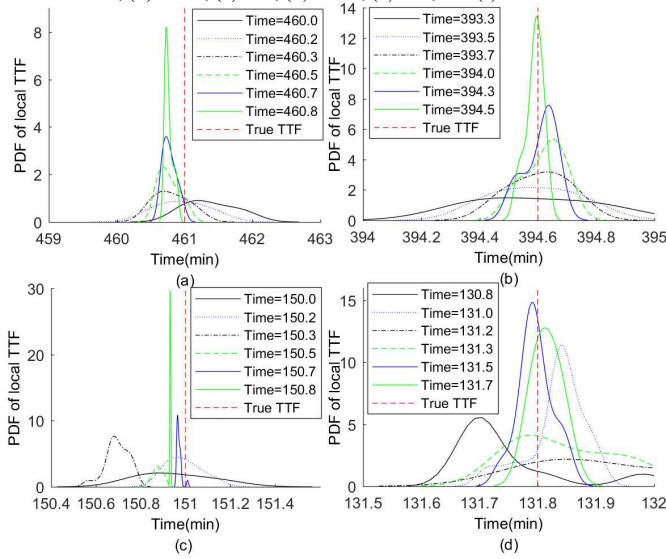
Fig. 10. Probability density function of local TTF at the different sampling times for (a) REB 1_1, (b) REB 1_3, (c) REB 2_1, and (d) REB 2_2.
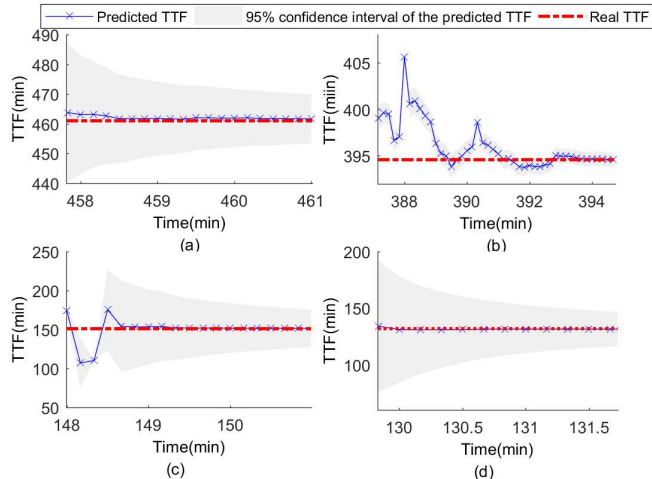
Fig. 11. Global TTF and its 95% confidence interval for (a) REB 1_1, (b) REB 1_3, (c) REB 2_1, and (d) REB 2_2.

The error of TTF prognostics is given as:

$$E_r(\%) = 100 * \left| \frac{t_{failure} - \hat{t}_{failure}}{t_{failure}} \right| \qquad (37)$$

where $t_{failure}$ and $\hat{t}_{failure}$ are the real and predicted TTFs of the tested REBs, respectively.

Similar experiments with the scheme of TTF prediction were also performed using other approaches in literatures. Table III

shows a comparison of the predicted results between the proposed approach and the existing major approaches. It is found in Table III that the proposed approach achieves much better prediction accuracy than SVM [7], hidden semi-Markov model [25], TFR-LDA [26], MoG-HMM [27], extended KF [28], and Gaussian mixture model [29]. This clearly shows the superiority of the proposed approach over the existing major approaches. This is because the proposed approach makes most of the dependence between degradation data over time.

TABLE Ⅲ
COMPARISON OF PREDICTED RESULTS BETWEEN PROPOSED APPROACH AND EXISTING MAJOR APPROACHES

Method	Errors (%)			
	Bearing 1_1	Bearing 1_3	Bearing 2_1	Bearing 2_2
Proposed approach	0.02	0.86	0.22	0.37
Cartella *et al.* [25]	37.72	12.62	27.18	18.1
Zhao *et al.* [26]	13.9	30.1	47.2	17.3
Medjaher *et al.* [27]	21.3	12.1	N/A	N/A
Soualhi *et. al.* [7]	0.6	1.25	N/A	N/A
Singleton *et al.* [28]	N/A	30.57	N/A	N/A
Chen *et al.* [29]	N/A	31.92	N/A	N/A

IV. CONCLUSIONS

This paper has proposed a new three-step degradation data-driven TTF prognostics approach of REBs in electrical machines. In this approach, the first step is to extract multiple degradation features, including statistical features computed by time-domain and frequency-domain analyses, intrinsic energy features reckoned by CEEMDAN time-frequency analyses, and fault frequency features calculated by HHT time-frequency analyses. In the second step, the degradation features, which are monotonic, robust, and correlative to the fault evolution of the REBs, are selected and fused into a PCMD health index using DPCA and Mahalanobis distance methods. The degradation time of the REBs might be discovered in accordance with the obtained PCMD health index. In the third step, a series of local degradation trajectory are generated using exponential regression, and the corresponding local TTF observations are obtained. On this basis, an empirical Bayesian algorithm is introduced to realize the global TTF prediction. Unlike the common way, the TTF prediction is continuously updated. In the experimental demonstration, the results illustrate that the proposed approach achieves good performance of TTF prediction, and exhibits great superiority over the existing major approaches.

It should be mentioned that degradation threshold and failure threshold have influenced the accuracy of TTF prognostics, which are subjectively set. Little research has been implemented on adaptively setting the thresholds in TTF prognostics. In the future, we will investigate adaptive threshold setting approaches.

REFERENCES

[1] A. Heng and S. Zhang, "Rotating machinery prognostic: State of the art, challenges and opportunities," Mech. Syst. Signal Process., vol. 23, no. 6, pp. 724-739, Apr. 2009.

[2] L. Liao, "Discovering prognostic features using genetic programming in remaining useful life prediction," IEEE Trans. Ind. Electron., vol. 61, no. 5, pp. 2464–2472, May 2014.

[3] S. Yin, X. Li, H. Gao, and O. Kaynak, "Data-based techniques focused on modern industry: An overview," IEEE Trans. Ind. Electron., vol. 62, no. 1, pp. 657-667, Jan. 2015.

[4] R. K. Singleton, E. G. Strangas, and S. Aviyente, "Extended Kalman filtering for remaining-useful-life estimation of bearings," IEEE Trans. Ind. Electron., vol. 62, no. 3, pp. 1781–1790, Mar. 2015.

[5] K. Javed, R. Gouriveau, N. Zerhouni, and P. Nectoux, "Enabling health monitoring approach based on vibration data for accurate prognostics," IEEE Trans. Ind. Electron., vol. 62, no. 1, pp. 647-656, Jan. 2015.

[6] M. H. Wei, M. Y. Chen, and D. H. Zhou, "Multi-sensor information based remaining useful life prediction with anticipated performance, " IEEE Trans. Rel., vol. 62, no. 1, pp. 183-198, Mar. 2013.

[7] A. Soualhi, K. Medjaher, and N. Zerhouni, "Bearing health monitoring based on Hilbert–Huang transform, support vector machine, and regression," IEEE Trans. Instrum. Meas., vol. 64, no. 1, pp. 52-62, Jan. 2015.

[8] J. Tian, C. Morillo, M. H. Azarian, and M. Pecht, "Motor bearing fault detection using spectral Kurtosis-based feature extraction coupled with K-nearest neighbor distance analysis," IEEE Trans. Ind. Electron., vol. 63, no. 3, pp. 1793-1803, Mar. 2016.

[9] Y. H. Wang, C. Deng, J. Wu, and Y. Xiong, "Failure time prediction for mechanical device based on the degradation sequence," J. Intell. Manuf., vol. 26, no. 6, pp. 1181-1199, 2015.

[10] W. H. Li, S. H. Zhang, and G. L. He, "Semisupervised distance-preserving self-organizing map for machine-defect detection and classification," IEEE Trans. Instrum. Meas., vol. 62, no. 5, pp. 869-879, May 2013.

[11] B. Zhang, C. Sconyers, C. Byington, R. Patrick, M. E. Orchard, and G. Vachtsevanos, "A probabilistic fault detection approach: application to bearing fault detection," IEEE Trans. Ind. Electron., vol. 58, no. 5, pp. 2011-2018, May 2011.

[12] A. Soualhi, H. Razik, G. Clerc, and D. D. Doan, "Prognosis of Bearing Failures Using Hidden Markov Models and the Adaptive Neuro-Fuzzy Inference System," IEEE Trans. Ind. Electron., vol. 61, no. 6, pp. 2864-2874, Jun. 2014.

[13] D. Tobon-Mejia, K. Medjaher, N. Zerhouni, and G. Tripot, "A data-driven failure prognostics method based on mixture of Gaussians hidden Markov models," IEEE Trans. Rel., vol. 61, no. 2, pp. 491-503, Jun. 2012.

[14] Y. H. Wang, C. Deng, J. Wu, Y. C. Wang, and Y. Xiong, "A corrective maintenance scheme for engineering equipment," Engineering Failure Analysis, vol. 36, pp. 269-283, 2014.

[15] R. Khelif, B. Chebel-Morello, S. Malinowski, E. Laajili, "Direct remaining useful life estimation based on support vector regression," IEEE Trans. Ind. Electron., vol. 64, no. 3, pp. 2276-2284, Mar. 2017.

[16] Y. B. Li, M. Q. Xu, X. H. Liang, W. H. Huang, "Application of bandwidth EMD and adaptive multiscale morphology analysis for incipient fault diagnosis of rolling bearings," IEEE Trans. Ind. Electron., vol. 64, no. 8, pp. 6506-6517, Jan. 2017.

[17] S. Osman, and W. Wang, "A morphological Hilbert-Huang transform technique for bearing fault detection," IEEE Trans. Instrum. Meas., vol. 65, no. 11, pp. 2646-2656, Nov. 2016.

[18] E. Elbouchikhi, V. Choqueuse, Y. Amirat, M. E. H. Benbouzid, and S. Turri, An efficient Hilbert-Huang transform-based bearing faults detection in induction machines," IEEE Trans. Energy Convers., vol. 32, no. 2, pp. 401-413, Jun. 2017.

[19] T. W. Rauber, F. A. Boldt, and F. M. Varejão, "Heterogeneous feature models and feature selection applied to bearing fault diagnosis," IEEE Trans. Ind. Electron., vol. 62, no. 1, pp. 637-646, Jan. 2015.

[20] J. Wu, C. Y. Wu, Y. Q. Lv, C. Deng, X. Y. Shao, "Design a degradation condition monitoring system scheme for rolling bearing using EMD and PCA," Industrial Management & Data Systems, vol. 117, no. 4, pp.713-728, 2017.

[21] J. B. Yu, "Health condition monitoring of machines based on hidden Markov model and contribution analysis," IEEE Trans. Instrum. Meas., vol. 61, no. 8, pp. 2200-2211, Aug. 2012.

[22] N. Z. Gebraeel, M. A. Lawley, R. Li, J. K. Ryan, "Residual-life distributions from component degradation signals: a Bayesian approach," IIE Trans., vol. 37, no. 6, pp. 543-557, Feb. 2015.

[23] P. Nectoux, et al., "Pronostia: an experimental platform for bearings accelerated degradation tests," in Proc. IEEE Int. Conf. on Prognost. Health Manage., 2012, pp. 1-8.

[24] A. Allahyar, H. S. Yazdi, A. Harati, "Constrained semi-supervised growing self-organizing map," Neurocomputing, vol. 147, no. 5, pp. 456-471, Jan. 2015.

[25] F. Cartella, J. Lemeire, and L. Dimiccoli, "Hidden Semi-Markov Models for predictive maintenance,"Mathe. Prob. in Engineering. vol. 2015, pp. 1-23, Dec. 2015.

[26] M. Zhao, B. Tang, and Q. Tan, "Bearing remaining useful life estimation based on time-frequency representation and supervised dimensionality reduction," Measurement, vol. 86, pp. 41-55, Feb. 2016.

[27] K. Medjaher, D. A. Tobon-Mejia and N. Zerhouni, "Remaining useful life estimation of critical components with application to bearings," IEEE Trans. Rel., vol. 61, no.2, pp. 292-301, Jun. 2012.

[28] R. K. Singleton, E, G. Strangas, and S. Aviyente, "Time-frequency complexity based bearings useful life (RUL) estimation for bearing faults," in IEEE Conf. Diag. for Elc. Machines, pp. 600-606, Aug. 2013.

[29] J. Chen, X. Wang, W. Zhou, L. Zhang, and F. Liu, "Multiple health phases based remaining useful lifetime prediction on bearings," Lecture Notes in Computer Science, vol. 9728, pp. 110-124, Jun. 2016.

Jun Wu received his B.S. degree from Hubei University of Technology, China, in 2001, and received his M.S. and Ph.D. degrees in mechanical engineering from Huazhong University of Science and Technology (HUST), in 2004 and 2008, respectively. He is currently an Associate Professor of School of Naval Architecture and Ocean Engineering at HUST. He worked as a visiting scholar at Stanford University, CA, USA from 2014 to 2015, where he conducted technical research in the area of structure health monitoring. His research interests include equipment health monitoring, fault diagnosis and remaining useful life prediction. He has more than 50 publications and the award of 9 patents, and receives several awards for his teaching activities.

Chaoyong Wu received his B.S. degree in mechanical engineering from Wuhan Textile University, China, in 2014 and his M.S. degree from Huazhong University of Science and Technology in 2017. His research interests include health monitoring and remaining useful life prediction for equipment.

Shuai Cao received his B.S. degree from Jiangsu University of Science and Technology, China, in 2015. He is currently working toward the M.S. degree at School of Naval Architecture and Ocean Engineering, Huazhong University of Science and Technology. His research interests include health monitoring and remaining useful life prediction for equipment.

Siu Wing Or received his B.Sc., M.Phil., and Ph.D. degrees in engineering physics from The Hong Kong Polytechnic University (PolyU) in 1995, 1997, and 2001, respectively. He worked as a Postdoctoral Research Fellow in the Mechanical and Aerospace Engineering Department at the University of California, Los Angeles, USA, for 1.5 years before he joined PolyU as a Lecturer in 2002. He is currently a Full Professor in the Department of Electrical Engineering, the Director of Smart Materials and Systems Laboratory, and the Director of Electrical Protection and High Voltage Coordination Laboratory at PolyU. His research interests include smart materials and devices in the bulk, micro-, and nano-scale, condition and structural health monitoring, energy harvesting and storage, electromagnetics, ultrasonics, and vibration control. He has more than 300 publications, including 2 professional book chapters, more than 200 SCI journal papers, more than 60 international conference papers, in addition to the award of 43 patents. Prof. Or is a senior member of IEEE.

Chao Deng received her B.S. degree from Wuhan University of Technology in 1992 and Ph.D. degree from Huazhong University of Science and Technology (HUST) in 1998. She is currently a Full Professor of School of Mechanical Science and Engineering at HUST. Prior to joining HUST in 2001, she worked as a postdoctoral research fellow at the Tokyo Institute of Technology, Japan, where she conducted technical research in the area of life cycle assessment. She has research interests in quality management and reliability engineering. She has published more than 80 research papers and received several awards for her teaching activities.

Xinyu Shao received his B.S., Ph.D. degrees in mechanical engineering from Huazhong University of Science and Technology (HUST), in 1990 and 1998, respectively. He was a visiting Ph.D. candidate with the Department of Industrial and Manufacturing Systems Engineering, University of Michigan–Dearborn, Dearborn, MI, USA, from 1995 to 1998. He is currently a Full Professor with the School of Mechanical Science and Engineering, HUST. He is also the Director of the National Engineering Research Center for the Digitization of Manufacturing Equipment. His research interests include digital and intelligent manufacturing, concurrent engineering, and quality/reliability engineering. He was a recipient of the Ministry of Education's Chang Jiang Scholars Program Professor in 2004, the National Science Fund for Distinguished Young Scholars in 2008, and the Second-Grade State Scientific and Technological Progress Prizes in 2001, 2008, and 2012.